Journal of Power Sources 196 (2011) 5102–5108

Contents lists available at ScienceDirect

Journal of Power Sources

journal homepage: www.elsevier.com/locate/jpowsour

Aging of $LiNi_{1/3}Mn_{1/3}Co_{1/3}O_2$ cathode material upon exposure to H_2O

Xiaoyu Zhang[a,c], W.J. Jiang[b], X.P. Zhu[b], A. Mauger[a,*], Qilu[c], C.M. Julien[d]

[a] Institut de Minéralogie et de Physique des Milieux Condensée, Université Pierre et Marie Curie, 140 rue de Lourmel, 75015 Paris, France
[b] CITIC Guoan Mengguli Power Source Technology Co. Ltd., Beijing 102200, PR China
[c] Department of Applied Chemistry, College of Chemistry and Molecular Engineering, Peking University, Beijing 100871, PR China
[d] PECSA, Université Pierre et Marie Curie, 4 place Jussieu, 75005 Paris, France

ARTICLE INFO

Article history:
Received 12 October 2010
Received in revised form
20 December 2010
Accepted 2 February 2011
Available online 15 February 2011

Keywords:
Li-ion batteries
Lamellar compounds
Surface aging

ABSTRACT

$LiNi_{1/3}Mn_{1/3}Co_{1/3}O_2$ compound was successfully synthesized by the co-precipitation method. The effect of H_2O on $LiNi_{1/3}Mn_{1/3}Co_{1/3}O_2$ in humid atmosphere was investigated by structural, magnetic and electrochemical analysis, and Raman spectroscopy. The consequence is that immersion of $LiNi_{1/3}Mn_{1/3}Co_{1/3}O_2$ to H_2O and exposure of $LiNi_{1/3}Mn_{1/3}Co_{1/3}O_2$ to humid atmosphere (ambient atmosphere, 20 °C, 50% relative humidity) led to a rapid attack that manifests itself by the delithiation of the surface layer of the particles and the concomitant formation of LiOH and Li_2CO_3 at the surface. This aging process occurred during the first few minutes, then it is saturated, and the thickness of the surface layer at saturation is 10 nm. After aging, an initial discharge capacity of 139 mAh/g was delivered at 1C-rate in the cut-off voltage of 3.0–4.3 V. About 95% of its initial capacity was retained after 30 cycles.

1. Introduction

The layered transition-metal oxide $LiNi_{1/3}Mn_{1/3}Co_{1/3}O_2$ seems very promising to replace $LiCoO_2$ for rechargeable Li-ion batteries, due to its higher reversible capacity with milder thermal stability at charged state, lower cost and less toxicity than $LiCoO_2$ [1–4]. However, the extensive use of $LiNi_{1/3}Mn_{1/3}Co_{1/3}O_2$ requires investigation of the stability of this material. Abuse tolerance is known to be an important parameter for industrial applications, because protections for Li-ion batteries are expensive. Tolerance upon exposure to humidity is also an important parameter as it conditions the storage for the material.

The lamellar compounds and actually all the cathode elements have to some extent a hygroscopic character. That of $LiNi_{0.83}Co_{0.15}Al_{0.005}O_2$ has been investigated in [5]. When this material is exposed to air with relative humidity 50% for 48 h, the moisture content was 1270 ppm. When this air-exposed material was heat-treated at 700 °C for 2 h, the moisture content in the powder decreased to 250 ppm, but its value increased to 2576 ppm after being exposed to air again. The moisture content measured for $LiCoO_2$ is in the range 100–300 ppm [5]. This hygroscopic character is not specific to lamellar compounds, and has also been observed in olivine $LiFePO_4$ for instance [6]. The phenomenon is due to the high reactivity of Li with H_2O, which is responsible for the complete delithiation of the surface layer over a thickness of few nanometers.

The lithium that is removed from the surface layer forms other Li-compounds that have also been observed, such as LiOH in case of $LiFePO_4$ exposed to air for a rather short period of time (few days), or Li_2CO_3 in case of longer time of exposure (few months) [6]. The same holds true for $LiNiO_2$ [7]. For $LiNi_{0.8}Co_{0.15}Al_{0.005}0_2$ powder also, since the long-term exposure to air produced a dense Li_2CO_3 coating approximately a few nm thick, which severely reduces the capacity in an irreversible manner [8]. The exposure to moisture has been also investigated in $LiNi_{1-x-y}Co_xMn_yO_2$. For $1-x-y>0.8$, the rapid reaction of this product with air also results in the formation of LiOH and Li_2CO_3 and on the surface [8–10]. In the present work, we used Raman spectroscopy to determine the nature of the impurities formed on the surface by the lithium that has been removed from the surface layer, since this technique that does not require measurements under vacuum is best suited for *in situ* investigation of the surface degradation upon exposure to ambient atmosphere. We find that both LiOH and Li_2CO_3 are formed at the surface of $LiNi_{1/3}Mn_{1/3}Co_{1/3}O_2$ even for short time of exposure, which extends to a broader range of concentration the sensitivity of $LiNi_{1-x-y}Co_xMn_yO_2$ reported for $1-x-y>0.8$, since $1-x-y=1/3$ in our case.

In our prior work on $LiFePO_4$, the remarkable sensitivity of magnetic experiments made them a very useful tool to quantify this reactivity to H_2O in the ambient air, since the delithiation of the surface layer imposes that all the iron ions in it change their valence from Fe^{2+} to Fe^{3+}, and these ions do not carry the same

* Corresponding author. Tel.: +33 144274439; fax: +33 144273882.
E-mail address: alain.mauger@impmc.jussieu.fr (A. Mauger).

0378-7753/$ – see front matter © 2011 Elsevier B.V. All rights reserved.
doi:10.1016/j.jpowsour.2011.02.009

magnetic moment. The same holds true in the lamellar compounds $LiNi_{1/3}Mn_{1/3}Co_{1/3}O_2$, except that it is now the nickel ions that switch to the Ni^{4+} valence state in the surface layer. In the present work, we use this effect to extend our prior analysis of $LiFePO_4$ to $LiNi_{1/3}Mn_{1/3}Co_{1/3}O_2$, which makes possible a more quantitative comparison between the sensitivity of this lamellar and the olivine compound to exposure to humidity. For this purpose, we have explored the reactivity of $LiNi_{1/3}Mn_{1/3}Co_{1/3}O_2$ to H_2O by investigating the evolution of the magnetic and optical properties of $LiNi_{1/3}Mn_{1/3}Co_{1/3}O_2$ upon exposure to moisture (ambient air 20 °C, 60% humidity) and the correlated degradation of the electrochemical properties. Our results confirm the general trend that the lamellar compounds are more sensitive than the olivine compounds to humidity.

2. Experimental

2.1. Sample synthesis and aging process

The synthesis of $LiNi_{1/3}Mn_{1/3}Co_{1/3}O_2$ powder was performed by a hydroxide route, using transition-metal hydroxide and lithium carbonate as starting materials. Two samples, say A and B, were synthesized, which differ by the initial lithium over metal ratio Li/M (with M = Ni + Mn + Co) in the precursors. The samples investigated in this work are the samples named A and B in Ref. [11], obtained after firing at 950 °C for 10 h, with Li/M = 1.05 for sample A and Li/M = 1.10 for sample B. The detailed information on the synthesis (choice of precursors, procedure) can be found in Ref. [11]. Reactivity to humidity has been studied by using the following procedures in two steps. First, make immersion of 1 g of pristine powder into 100 ml distilled water and mix them at room temperature with continuous magnetic stirring for different periods of time (15 min, 30 min, 2 h, 17 h). Then evaporate the water and dry at 120 °C to get the final powder. Second, put the powder in the humid atmosphere (ambient air at 20 °C, 60% relative humidity) for different periods of time (1 day, 1 week, 1 month). However, as we shall see, no change has been detected during the second step, and the aging of the particles only occurs during the immersion in water during the first 15 min.

The aging has been characterized by measurements of the magnetic and optical properties. All the details on the apparatus that have been used can be found in Ref. [11]. The temperature dependence of the susceptibility data was recorded during heating of the sample using two modes: zero field cooling (ZFC) and field cooling (FC), to determine the magnetic behavior. The procedure is based on performing two consecutive magnetization measurements: in ZFC the sample is first cooled down in the absence of magnetic field, then a magnetic field H = 10 kOe is applied, and the ZFC magnetic susceptibility $M(T)/H$ where M is the magnetization is measured upon heating. In the FC experiments, the same magnetic field is applied first at room temperature; the FC susceptibility is measured upon cooling.

2.2. Electrochemistry

The electrochemical properties were tested at room temperature in cells with metallic lithium as anode electrode. Charge–discharge tests were performed on coin type cell (CR2032). Composite positive electrode was prepared by thoroughly mixing the active material (90 wt%) with carbon black (2 wt%), acetylene black (2 wt%), polyvinylidene fluoride (6 wt%) in N-methyl-pyrrolidinone and spread onto aluminium foils then dried for 24 h at 120 °C in vacuum. Cells were then assembled in an argon-filled glove box (Braun, Germany) using foils of Li metal as counter electrode and Celgard 2400 as separator. The electrolyte was 1.0 mol L^{-1} $LiPF_6$ in a mixture of ethylene carbonate (EC) and diethyl carbonate (DEC) (1:1, v/v). The cells were galvanostatically cycled between 3.0 V and 4.3 V versus Li^0/Li^+ on a Land CT2001A battery tester (China, Wuhan Jinnuo Electronics Co. Ltd) at room temperature.

Table 1
Lattice parameters a, c, c/a, V of two samples of $Li_{1+x}(Ni_{1/3}Mn_{1/3}Co_{1/3})_{1-x}O_2$ (x = 0.02, 0.04) before and after aging.

Sample	a(Å)	c(Å)	c/a	V(Å^3)
A	2.8650(1)	14.252(2)	4.9745(9)	101.31(2)
A-aging	2.8642(1)	14.250(3)	4.9752(8)	101.25(3)
B	2.8603(2)	14.241(2)	4.9788(10)	100.90(3)
B-aging	2.8604(2)	14.238(1)	4.9776(7)	100.88(2)

3. Results and discussion

3.1. Structural analysis

The samples A and B have been characterized by inductively coupled plasma (ICP) spectroscopy and X-ray diffraction. The results, together with the Rietveld refinements for both samples have been reported in Ref. [11]. To summarize the results reported in this earlier work (Table 1 in Ref. [11]), we found that the molar ratio of the final product is within 1% for all the components, corresponds to the formula $Li_{1+x}(Ni_{1/3}Mn_{1/3}Co_{1/3})_{1-x}O_2$ with x = 0.020(4) and 0.040(4) for samples A and B, respectively.

As seen in Fig. 1a and b, the Bragg lines are well indexed in the $R\bar{3}m$ space group with the hexagonal ordering. No impurity phases are detected and the powders are well crystallized in the α-

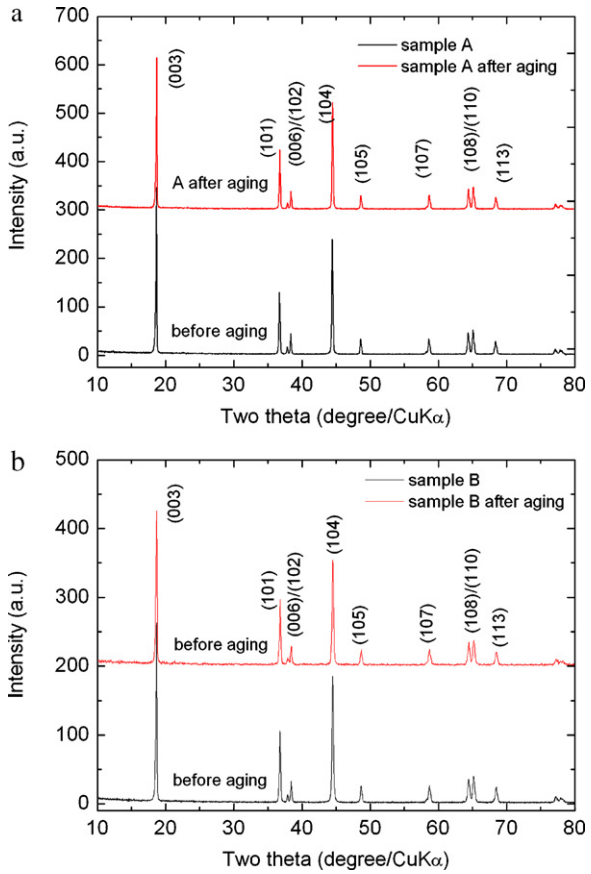

Fig. 1. XRD patterns of $Li_{1.02}(Ni_{1/3}Mn_{1/3}Co_{1/3})_{0.98}O_2$ before and after aging for samples A and B.

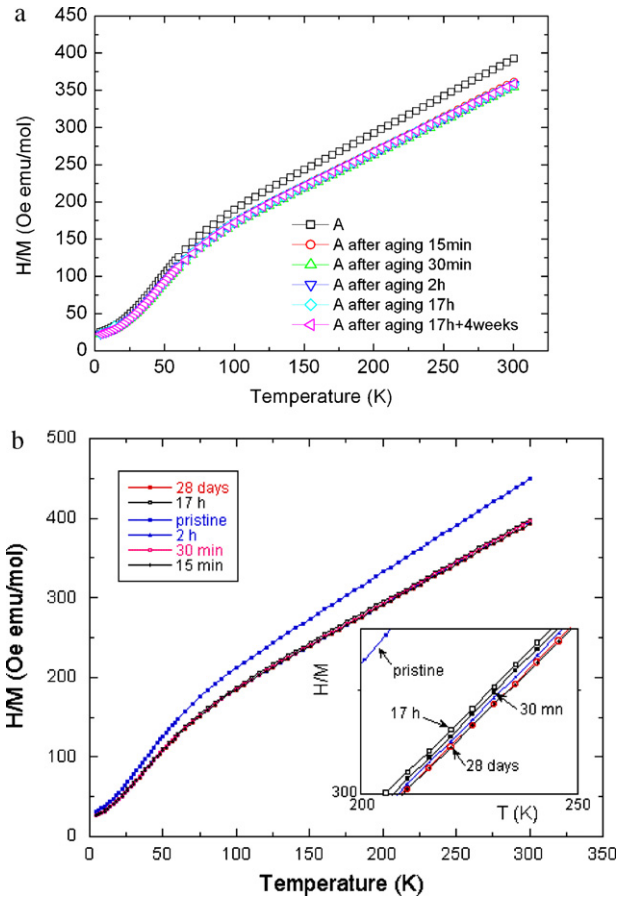

Fig. 2. Plot of the reciprocal magnetic susceptibility H/M before aging and after aging for different periods of time for sample A (a) and B (b). Data were collected with a magnetic field $H = 10$ kOe. After aging 17 h + 4 weeks means that the material has been immersed for 17 h in water before drying, then dried and left 4 weeks at room temperature in ambient atmosphere humidity. The insert in (b) is an enlargement to show the difference at different times of exposure.

$NaFeO_2$ type structure [12,13]. The (0 0 6)/(1 0 2) and (1 0 8)/(1 1 0) doublets are both well separated, which indicate a good hexagonal ordering of $Li_{1+x}(Ni_{1/3}Mn_{1/3}Co_{1/3})_{1-x}O_2$ after aging process [14,15]. The narrow diffraction peaks of the pattern indicate a high crystallinity of the powders and suggest a homogeneous distribution of the cations within the structure [16]. Let us also recall that the lattice coherence length in the plane perpendicular to the c-axis is 59.4(4) nm and that the mean crystallite size along the c-axis is 8 nm larger than in the perpendicular direction Ref. [11]. This elongated shape of the crystallites is correlated to the anisotropic shape of the particles observed by SEM for both samples [11]. The lattice parameters of synthesized samples were obtained by least-square method and the results were summarized in Table 1. There is no big difference in lattice parameters of the samples after aging, which means that the exposure to humidity only affect the surface layer of $Li_{1+x}(Ni_{1/3}Mn_{1/3}Co_{1/3})_{1-x}O_2$. We will determine its thickness by magnetic measurements that are more sensitive than XRD [6].

3.2. Magnetic analysis

The temperature dependence of the reciprocal magnetic susceptibility, $\chi_m^{-1} = H/M$ is presented in Fig. 2a and b for the two samples before aging, and after aging for different periods of time. Above 150 K, the curve $\chi_m^{-1}(T)$ shows a paramagnetic (PM) behavior and the magnetization is linear in field for all the samples, so that χ_m^{-1} is meaningful, i.e. $M/H = dM/dH$. The quasi-linear variations of χ_m^{-1} with T at the susceptibility can be described by a Curie–Weiss law

Table 2
Magnetic properties of two samples before and after aging, i.e. after immersion in water during a time $t \geq 15$ min.

Samples	C_p(emu K/mol)	Θ_p (K)	μ_{eff} (μ_B) (±0.01)	Cation mixing (%)
A before aging	0.99	−89	2.83	1.88
A after aging	1.08	−87	2.96	1.89
B before aging	0.85	−80	2.62	1.50
B after aging	0.95	−79	2.77	1.52

$\chi_m^{-1} = (T - \Theta_p)/C_p$, with Θ_p the Curie–Weiss temperature, and C_p the Curie constant related to the effective magnetic moment μ_{eff} by the relation $C_p = N\mu_{eff}^2/3k_B$ with k_B the Boltzmann constant and N the number of metal ions in one mole of product. The values of the two fitting parameters Θ_p and μ_{eff} obtained are reported in Table 2. The accuracy on Θ_p is ±1 K (i.e. slightly larger than 1%). The relative error on the magnetic moment μ_{eff} is smaller, because Θ_p is determined by extrapolation of the Curie–Weiss law from the range 100–300 K to −90 K, while μ_{eff} results from the measurement of the slope of the linear $\chi^{-1}(T)$ law [17]. In addition, this slope is in μ_{eff}^2, which reduces the relative error on μ_{eff} by a factor 2. As a consequence, the absolute error on the values of μ_{eff} in Table 2 is ±0.01. Θ_p is negative in all compounds and this is an intrinsic property due to the fact that intrinsic magnetic interactions are mainly the intra-layer super-exchange interactions mediated via oxygen at 90° bonding angle, which are dominantly antiferromagnetic according to the Goodenough rules [18–22]. In addition, the experimental value of the effective magnetic moment μ_{eff} of samples A and B after aging in the paramagnetic regime increase to 2.96 μ_B and 2.77 μ_B, respectively. But when the aging time increases (from 15 min to 17 h), μ_{eff} does not change significantly anymore (see Fig. 2). Therefore, the immersion in water has important effects on the magnetic properties, but during the first 15 min only. The magnetization curves do not change upon longer times of immersion.

We attribute the increase of μ_{eff} upon exposure to humidity to the delithiation of a surface layer over a thickness d. Due to the excess of lithium (in concentration $x = 0.02$ instead of 0.00), the electrical neutrality implies that there are $2x$ nickel ions in the trivalent state (low spin state $S = 1/2$) [11]. Due to the very strong reactivity of Li to humidity, not only for metal Li, but also for Li in intercalation compounds [6], we can assume that the delithiation in the surface layer has reached the situation where all the Ni^{2+} ions and Ni^{3+} ions have been converted in Ni^{4+} ions. Take sample A as an example, the effective moment for sample A is $\mu_1 = 2.83\ \mu_B$ before aging, increasing to $\mu_2 = 2.96\ \mu_B$ after aging. Let us recall that the magnetic moments carried by Ni^{2+} and Ni^{4+} are $\mu_{Ni}{}^{2+} = 2.83\ \mu_B$ and $\mu_{Ni}{}^{4+} = 4.90\ \mu_B$. Let f_{Ni} be the fraction of Ni^{2+} and Ni^{3+} converted to Ni^{4+} upon delithiation. Taking into account that the amount of Ni^{2+} is $[(1-x)/3 - 2x] = 0.287$, and the amount of Ni^{3+} is $2x = 0.04$ for sample A, we find:

$$\mu_2^2 - \mu_1^2 = f_{Ni}[0.287(\mu^2_{Ni^{4+}} - \mu^2_{Ni^{2+}}) + 0.04(\mu^2_{Ni^{4+}} - \mu^2_{Ni^{3+}})] \quad (1)$$

The result is $f_{Ni} = 0.14$, which corresponds to a concentration of nickel converted to Ni^{4+} per mole $\Delta x = (0.287 + 0.04) f_{Ni} = 0.046$.

Since each mole of Ni^{2+} and of Ni^{3+} oxidized to Ni^{4+} requires 2 moles of Li^+ ions, and 1 mole of Li^+ ions, respectively, the fraction of Li lost during aging process is:

$$\eta = \frac{f_{Ni}(2 \times 0.287 + 0.04)}{1.02} \quad (2)$$

The result is $\eta = 0.08$. To relate this parameter to the thickness of the delithiated layer, we need the shape and size of the particles that can be deduced from the analysis of SEM image reported in Fig. 3. In first approximation, the primary particles are cylinders of width $D = 0.5\ \mu m$ and length $L = 2\ \mu m$, which corresponds to a

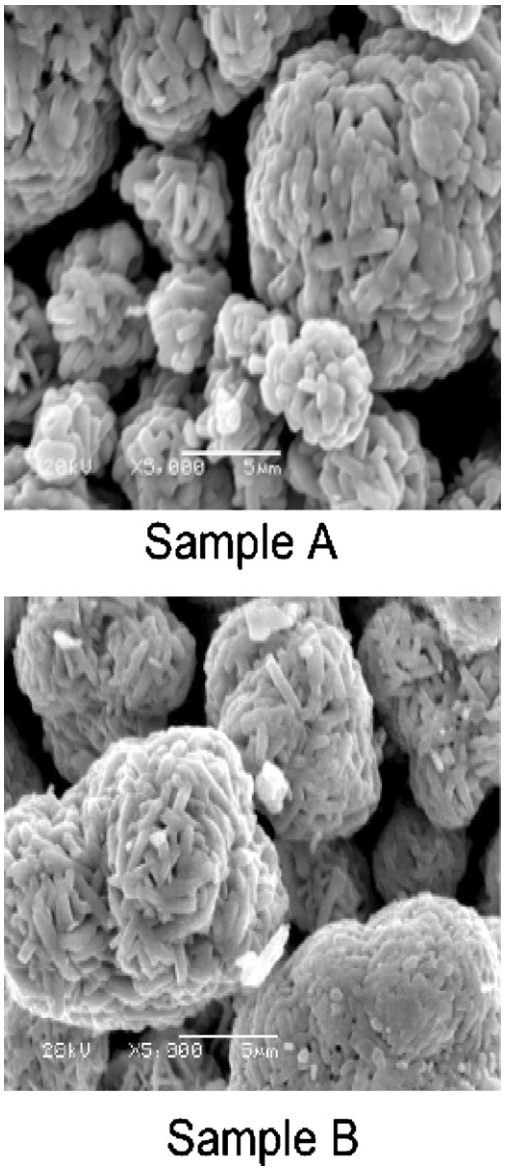

Fig. 3. SEM images of $Li_{1+x}(Ni_{1/3}Mn_{1/3}Co_{1/3})_{1-x}O_2$ samples A (up) and B (down).

volume of the primary particle $V = \pi D^2 L/4$. Let d be the thickness of the delithiated layer, so that the volume of the delithiated part of the particle is πDLd, and:

$$\eta = \frac{\pi DLd}{\pi D^2 L/4} = \frac{4d}{D} \quad (3)$$

From these equations, we find an estimate $d = 10$ nm for sample A. For sample B, the same calculation gives exactly the same value of η, and then of d since the size and shape of the particles is the same (see Fig. 3). This is the proof that the reaction to humidity is independent of the Li/M molar ratio.

The determination of f_{Ni} also allows us to determine the cation disorder. The concentration of Ni^{2+} on Li sites, i.e. $Ni^{2+}(3b)$ defects has been determined before aging in [11], from the analysis of magnetization curves $M(H)$ at low temperature. The magnetization curves after aging are reported in Fig. 4. The non-linearity of $M(H)$ at 4.2 K is due to the ferromagnetic spin freezing of the $Mn^{4+}(3a) - Ni^{2+}(3b)$ pair at low temperature. At 4.2 K where the magnetization of this pair is saturated, the effective spin of the pair is $S_{cl} = (S_{Mn} + S_{Ni}) = 5/2$, since the Mn^{4+} and Ni^{2+} ions carry a spin $S_{Mn} = 3/2$ and $S_{Ni} = 1$, respectively (and no orbital momentum, since

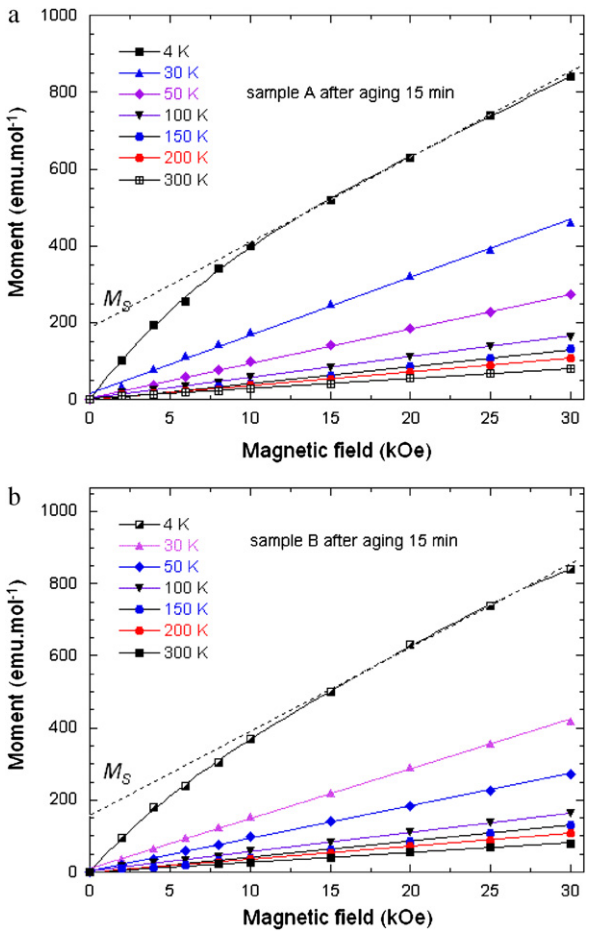

Fig. 4. Isothermal plots of the magnetization $M(H)$ after aging for samples A and B.

it is quenched by the crystal-field). This effective spin is easily saturated at 4.2 K by application of the magnetic field, and thus gives a contribution 5 μ_B to the magnetization at large value of H, giving rise to the magnetization M_S measured by extrapolation of $M(H)$ from large values of H to $H = 0$ (see Fig. 4). We can then estimate the amount of $Ni^{2+}(3b)$ defects as the ratio between M_S and the magnetization at saturation M_0 the sample would have if all the Mn and Ni ions were saturated ferromagnetically. This has been done in prior works [11,21,22] before aging. For sample A, for instance, the result before aging is a concentration $[Ni^{2+}(3b)] = 1.88\%$ and 1.50% for sample B [11]. In addition, we have shown in [11] that the results are in agreement with the $[Ni^{2+}(3b)]$ concentration deduced from Rietveld refinement. After aging, one has to calculate M_0. It can be deduced from the following formulas given per chemical formula for sample A, for which $[(1-x)/3 - 2x] = 0.287$ and the amount of Ni^{3+} is $2x = 0.04$:

$$\text{Concentration of } Ni^{4+}(\text{spin}S = 2) : 0.287 f_{Ni} + 0.04 f_{Ni}$$

$$\text{Concentration of } Ni^{2+}(\text{spin}S = 1) : 0.287 \times (1 - f_{Ni})$$

$$\text{Concentration of } Ni^{3+}(\text{spin}S = 3/2) : 0.04 \times (1 - f_{Ni})$$

$$\text{Concentration of } Mn^{4+}(\text{spin}S = 3/2) : (1-x)/3 = 0.327$$

Note that the Ni^{4+} is in the high-spin state in the surface layer. It should not be confused with the Ni^{4+} valence state that is formed inside the bulk, which is in the low-spin state. The spin state depends on the strength of the crystal field. The ion in the d^6 configuration is in the high-spin state if the crystal-field is small (this is

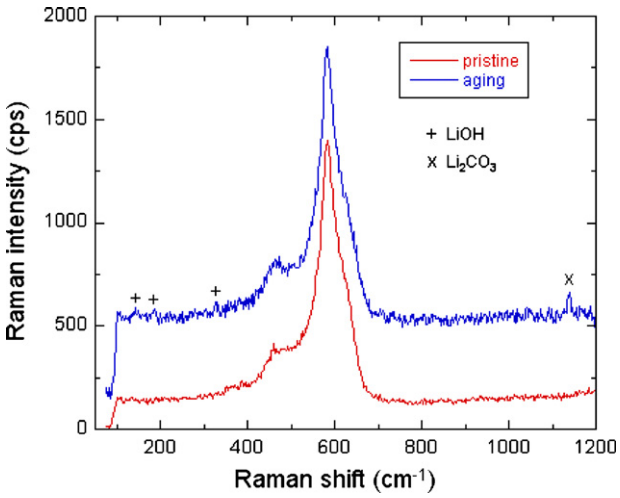

Fig. 5. Raman spectra of sample B in the pristine state, and after exposure to ambient atmosphere during 24 h.

the case of Fe^{2+} in $LiFePO_4$ for instance), and in the low-spin state in case the crystal field is strong enough so that the Hund's rule is violated. In $LiNi_{1/3}Mn_{1/3}Co_{1/3}O_2$, the surface relaxation weakens the crystal field in the surface layer, which results in this spin transition in the surface layer. Note a similar effect is also observed in $LiFePO_4$ since Fe^{3+} in the delithiated surface layer is either in the low-spin or high-spin state, depending on the surface state, except that it is a spin transition in the d^5 shell in this later case [23].

The value of M_0 deduced from these equations, taking into account that $f_{Ni} = 0.14$, and the value of $M_s = 186\,\text{emu/mol} = 0.0332\,\mu_B$ deduced for Fig. 4, give $[Ni^{2+}(3b)] = M_s/M_0 = 1.89\%$. This value is within experimental error equal to $[Ni^{2+}(3b)]$ before aging. This is also true for sample B (see Table 2), which shows that the defects are not involved in the aging process.

3.3. Raman spectroscopy

Raman spectroscopy has been used to determine which species have been formed by the lithium removed from the surface layer. The material has the spectroscopic D^5_{3d} symmetry, in which the vibration modes associated to each transition-metal ion are decomposed as follows:

$$\Gamma = 2A_{2u} + 2E_{2u} + A_{1g} + E_g. \quad (4)$$

Only the A_{1g} and E_g are Raman active modes. The A_{1g} and E_g modes originate from the M–O symmetrical stretching and O–M–O bending vibrations, respectively. Since the compound has three M-ions, we expect $3A_{1g}$ modes and $3E_g$ modes that overlap to give rise to the two broad A_{1g} and E_g structures in Fig. 5 for the pristine sample. The quantitative analysis of this Raman spectrum of pristine $LiNi_{1/3}Mn_{1/3}Co_{1/3}O_2$ has been reported in [21]. Upon exposure to ambient atmosphere for one day, the spectrum of the same sample shows three additional bands (markers "+" in the figure) that are characteristic of LiOH [6,23], and another band (marker "x") characteristic of CO_3 molecular unit [24], which confirms the presence of Li_2CO_3 in addition of the lithium hydroxide. We thus recover the general trend in intercalation compounds, whether they are lamellar or not, according to which the reaction of lithium with H_2O at the surface results in the delithiation of the surface layer, the lithium involved in the process forming LiOH and Li_2CO_3 at the surface.

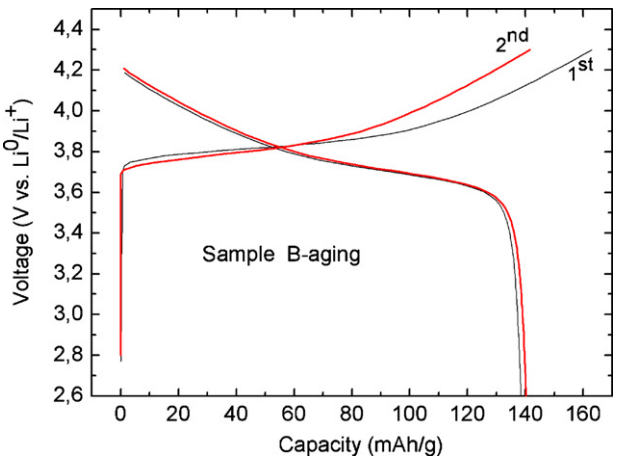

Fig. 6. Charge and discharge curves (1st, 2nd) of sample-B after aging.

3.4. Electrochemical analysis

The degradation of the surface of $LiNi_{1/3}Mn_{1/3}Co_{1/3}O_2$ affects the electrochemical properties of the material as a cathode element. Fig. 6 shows the charge and discharge curves for the first two cycles of sample B after aging with a constant current density of 1C rate (1C = 150 mA/g) between 3.0 and 4.3 V versus Li^0/Li^+ at room temperature. The first charge capacity and discharge capacity are 163 and 139 mAh/g, respectively. The irreversible capacity loss in the first cycle is 24 mAh/g and the coulombic efficiency is 85.3% (Fig. 7). The discharge capacity of sample B after aging reduced to about 93% of its pristine powder, due to delithiation during the aging process. After 30 cycles, the discharge capacity is 132 mAh/g and the capacity retention is 95% (Fig. 8). The same result before aging is also reported for comparison to emphasize the damage induced by exposure to water on the electrochemical properties. On another hand, the capacity loss does not significantly depend on the cycle number, and it corresponds to the fact that the capacity is reduced by the amount of lithium that has been removed in the 10 nm-thick surface layer upon exposure to humidity. It corroborates that the remaining part of the material is not significantly affected, and these results are self-consistent with the analysis of the magnetic properties of the previous section.

4. Discussion

In their work on $LiVO_2$, Manthiram and Goodenough [25] were the first to show the migration of lithium ions to the surface on exposing the layered oxides to moisture, and the consequent

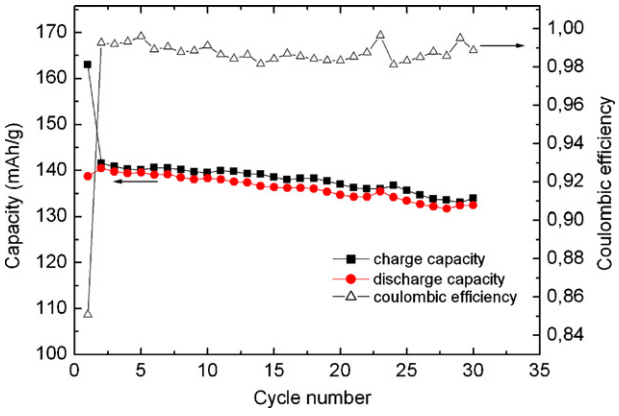

Fig. 7. Cycling performance and coulombic efficiency of sample-B after aging.

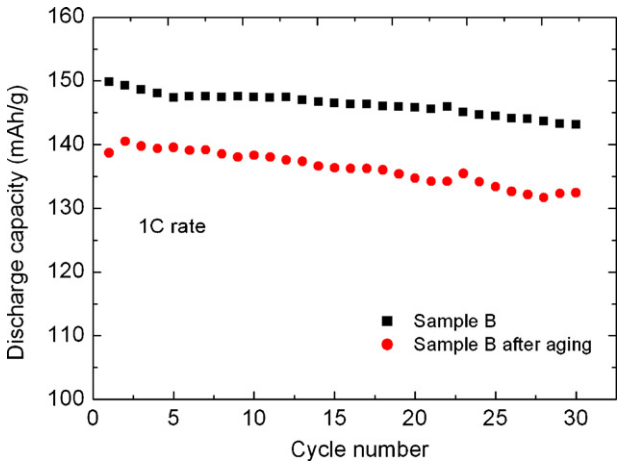

Fig. 8. Comparison of cycling performance of sample B before and after aging.

formation of Li_2CO_3. The presence of lithium carbonate on the surfaces of active cathode materials such as $LiNiO_2$ and its analogues $LiNi_{1-x-y}Co_xAl_yO_2$ has long been noted [26–35]. The surface of the particles in the present work has been characterized after a brief exposure to moisture. This is the reason why we have detected LiOH. The same holds true on the surface of other intercalation compounds, even if they are not lamellar, like $LiFePO_4$ [23]. On another hand, only Li_2CO_3 is observed after a long exposure in $LiNi_{0.8}Co_{0.15}Al_{0.05}O_2$ (two years in that case). Matsumoto et al. carried out a detailed study [31] of the reaction of $LiNi_{1-x-y}Co_xAl_yO_2$ with CO_2, and concluded that the formation of Li_2CO_3 is presumed to take place via reaction:

$$LiMO_2 + (z/4)O_2 + (z/2)CO_2 \rightarrow Li_{1-z}MO_2 + (z/2)Li_2CO_3, \quad (5)$$

according to which the rate of reaction was limited by diffusion of CO_2 through a dense surface layer of Li_2CO_3. Nevertheless, the presence of LiOH we have detected after a short time of exposure shows that the lithium carbonate is formed in a two-step process that is masked by Eq. (5). LiOH and Li_2O are formed by reaction with H_2O first, and are rapidly converted in Li_2CO_3 by reaction with CO_2 in a second step. This process accounts for the very rapid appearance of Li_2CO_3 on the surfaces of fresh samples following brief exposure to air.

It has been shown [36] that the air exposure of $LiNi_{0.8}Co_{0.15}Al_{0.05}O_2$ cathodes fabricated for use in high-power cells produces a large amount of Li_2CO_3 severely limits the performance of the electrodes by means of partial or complete isolation of active material by means of partial or complete isolation of active material. The same holds true in our case. The analogy with our results is even more striking. The thickness of the Li_2CO_3 coat has been estimated to 10 nm in $LiNi_{0.8}Co_{0.15}Al_{0.05}O_2$. This is the thickness of the delithiated layer that we have found in $LiNi_{1/3}Mn_{1/3}Co_{1/3}O_2$. Since the lithium that has been removed from the surface layer is entirely used to form Li_2CO_3 after Eq. (5), we expect that the thickness of Li_2CO_3 coat and that of the delithiated layer are about the same, which implies that the sensitivity to moisture is the same in $LiNi_{1-x-y}Co_xAl_yO_2$ and $LiMn_{1-x-y}Co_xAl_yO_2$. Of course, magnetic experiments are sensitive only to the change of the valence of the metal ion upon delithiation, so that we could only determine the thickness of the delithiated layer, while in [36], it was the opposite: the experimental tool was high resolution transmission microscopy that could detect only the Li_2CO_3 layer. In this sense, the present work can be considered as a complementary approach. The results also suggest that the sensitivity of $LiMO_2$ to moisture does not significantly depend on *M*.

The other feature hat we have observed in the present work is that the delithiated layer at the surface of the articles is stabilized after a very short time of exposure. Moreover, the lattice parameter remains unchanged, so that the delithiation occurs only in the surface layer. This can be understood if we note that the diffusion coefficient of the species involved in the reaction of Li with air is small. After the surface has been delithiated over a thickness of 10 nm, Li ions below this surface layer are too far from the surface to react with the air, and CO_2 is too far from them to diffuse and reach them. If, however, we give time to this diffusion process, the lithium ions will diffuse to homogenize the Li distribution. This diffusion process helps to conciliate our results with the variation of the lattice parameter observed in $LiNi_{0.8}Co_{0.15}Al_{0.05}O_2$ exposed to air during two years [36], or in $LiVO_2$ where surface-adsorbed oxidants extract lithium from the bulk up to the phase limit $Li_{0.7}VO_2$ [25].

The influence of the exposure to moisture on the electrochemical properties has been more controversial. It has been reported that Li_2CO_3 disappears from FT-IR spectra [37] of $LiCoO_2$ and $LiMn_2O_4$ electrodes and from X-ray photoelectron spectra [33] of $LiNi_{0.8}Co_{0.2}O_2$ cathode surfaces after cycling. A similar behavior in lightly contaminated $LiNi_{0.8}Co_{0.15}Al_{0.05}O_2$ electrodes stored or cycled in $LiPF_6$ EC/DEC (1:1) electrolyte [38]. However, more recent studies [36] have shown that, even after extended cycling and following overcharging to 4.3 V, Li_2CO_3 was still present in the heavily contaminated electrode, and the capacity loss was not recovered. We find the same result in the present work on $LiNi_{1/3}Mn_{1/3}Co_{1/3}O_2$, as the cycling did not lead to any improvement (see Fig. 8). Since the Li counter electrode is a reservoir of Li, one might have expected that a complete depth of discharge might have relithiated the surface layer, which is actually what we had observed in the case of $LiFePO_4$. We do not have this recovery here, which comforts the hypothesis proposed earlier [36], according to which partial isolation due to the Li_2CO_3 deposited on the surface of the active material is the mechanism for power and capacity losses.

5. Conclusion

The layered $Li_{1+x}(Ni_{1/3}Mn_{1/3}Co_{1/3})_{1-x}O_2$ compound was synthesized via co-precipitation method with different Li/*M* molar ratios. We have explored the reactivity of $LiNi_{1/3}Mn_{1/3}Co_{1/3}O_2$ to H_2O by investigating the evolution of the structural, magnetic and electrochemical properties of $LiNi_{1/3}Mn_{1/3}Co_{1/3}O_2$ upon exposure to moisture (ambient air 20 °C, 60% humidity). $Li_{1+x}(Ni_{1/3}Mn_{1/3}Co_{1/3})_{1-x}O_2$ compound is very sensitive to humidity. The aging process has important magnetic effect on powders and it occurs during the first few minutes only (then it saturates). The Li-ions that have reacted with H_2O have delithiated a surface layer to form at the surface LiOH and Li_2CO_3 detected by Raman spectroscopy. The thickness of the surface layer affected by this process can be estimated from the conversion of Ni^{2+} and Ni^{3+} to Ni^{4+} implied by this delithiation inside this layer, which can be detected by magnetic properties. The thickness of the surface layer is 10 nm, irrespective of the Li/*M* molar ratio. The presence of $[Ni^{2+}(3b)]$ defects does not affect this reaction to humidity either. The initial discharge capacity of sample B after aging is about 93% of that of its pristine powder and the capacity retention is 95% after 30 cycles. This material is then more sensitive to humidity than another cathode material, $LiFePO_4$. In this later case, we had determined that the delithiation process takes place in a layer of thickness 3 nm only, presumably because $FePO_4$ is waterproof [11]. This protection has been lost in $Li_{1+x}(Ni_{1/3}Mn_{1/3}Co_{1/3})_{1-x}O_2$, so that storage of this material in dry chamber is mandatory.

References

[1] T. Ohzuku, Y. Makimura, Chem. Lett. 30 (2001) 642.
[2] K.M. Shaju, G.V. Subba Rao, B.V.R. Chowdari, Electrochim. Acta 48 (2002) 145.
[3] N. Yabuuchi, Y. Koyama, N. Nakayama, T. Ohzuku, J. Electrochem. Soc. 152 (2005) A1434.
[4] Y. Koyama, N. Yabuuchi, I. Tanaka, H. Adachiand, T. Ohzuku, J. Electrochem. Soc. 151 (2004) A1545.
[5] J. Cho, Y. Kim, in: S.S. Zhang (Ed.), Advanced Materials and Methods for Lithium-Ion Batteries, Transworld Research Network Publ, 2007, p. 49.
[6] K. Zaghib, M. Dontigny, P. Charest, J.F. Labrecque, A. Guerfi, M. Kopec, A. Mauger, F. Gendron, C.M. Julien, J. Power Sources 185 (2008) 698.
[7] R. Moshtev, P. Zlatilova, S. Vasilev, I. Bakalova, A. Kozawa, J. Power Sources 21 (1999) 434.
[8] G.V. Zhuang, G. Chen, J. Shim, X. Song, P.N. Ross Jr., T.J. Richardson, J. Power Sources 134 (2004) 293.
[9] S.W. Song, G.V. Zhuang, P.N. Ross Jr., J. Electrochem. Soc. 151 (2004) A1162.
[10] K. Matsumoto, R. Kuzuo, K. Takeya, A. Yamanaka, J. Power Sources 81–82 (1999) 558.
[11] X.-Y. Zhang, W.-J. Jiang, A. Mauger, F. Qilu, C.M. Gendron, Julien, J. Power Sources 195 (2010) 1292.
[12] K. Ben Kamel, N. Amdouni, A. Abdel-Ghany, K. Zaghib, A. Mauger, F. Gendron, C.M. Julien, Ionics 14 (2008) 89.
[13] P.Y. Liao, J.G. Duh, S.R. Sheen, J. Electrochem. Soc. 152 (2005) A1695.
[14] T. Ohzuku, A. Ueda, M. Nagayama, Y. Iwakoshi, H. Komori, Electrochim. Acta 38 (1993) 1159.
[15] J.N. Reimers, E. Rossen, C.D. Jones, J.R. Dahn, Solid State Ionics 61 (1993) 335.
[16] K.S. Park, M.H. Cho, S.J. Jin, K.S. Nahm, Electrochem. Solid-State Lett. 7 (2004) A239.
[17] C.M. Julien, A. Ait-Salah, A. Mauger, F. Gendron, Ionics 12 (2006) 21.
[18] J.B. Goodenough, Magn. Chem. Bond, Wiley, New York, 1963.
[19] A. Abdel-Ghany, K. Zaghib, F. Gendron, A. Mauger, C.M. Julien, Electrochim. Acta 52 (2007) 4092.
[20] A. Abdel-Ghany, A. Mauger, F. Gendron, K. Zaghib, C.M. Julien, ECS Trans. 3 (2007) 137.
[21] X.Y. Zhang, A. Mauger Qilu, H. Groult, L. Perrigaud, F. Gendron, C.M. Julien, Electrochim. Acta 55 (2010) 6440.
[22] X.Y. Zhang, A. Mauger, F. Gendron, L. Qi, H. Groult, L. Perrigaud, C.M. Julien, ECS Trans. 16 (2009) 11.
[23] K. Zaghib, A. Mauger, F. Gendron, C.M. Julien, Chem. Mater. 20 (2008) 462.
[24] S. Okazaki, N. Ohtori, I. Okada, J. Chem. Phys. 91 (1989) 5587.
[25] A. Manthiram, J.B. Goodenough, Can. J. Phys. 65 (1987) 1309.
[26] T Ohzuku, A. Ueda, M. Nagayama, Y. Iwakoshi, H. Komori, Electrochim. Acta 38 (1993) 1159.
[27] J.G. Chen, B.D. Devries, J.T. Lewandowski, R.B. Hall, Catal. Lett. 23 (1994) 25.
[28] T. Nohma, H. Kurokawa, M. Uehara, M. Takahashi, K. Nishio, T. Saito, J. Power Sources 54 (1995) 522.
[29] C.C. Chang, N. Scarr, P.N. Kumta, Solid State Ionics 112 (1998) 329.
[30] G.T.K. Fey, Z.X. Weng, J.G. Chen, T.P. Kumar, Mater. Chem. Phys. 82 (2003) 5.
[31] K. Matsumoto, R. Kuzuo, K. Takeya, Yamanaka, J. Power Sources 81/82 (1999) 558.
[32] D. Aurbach, K. Gamolsky, B. Markovsky, G. Salitra, Y. Gofer, U. Heider, R. Oesten, M. Schmidt, J. Electrochem. Soc. 147 (2000) 1322.
[33] A.M. Andersson, D.P. Abraham, R. Haasch, S. MacLaren, J. Liu, K. Amine, J. Electrochem. Soc. 149 (2002) A1358.
[34] J.C. Badot, V. Bianchi, N. Baffier, N. Belhadj-Tahar, J. Phys. Condens. Matter 14 (2002) 6917.
[35] H.-K. Kim, T.-Y. Seong, W. Cho, Y.S. Yoon, J. Power Sources 109 (2002) 178.
[36] G.V. Zhuanga, G. Chenb, J. Shimb, X. Songb, P.N. Rossa, T.J. Richardson, J. Power Sources 134 (2004) 293.
[37] D. Aurbach, J. Power Sour 89 (2000) p206.
[38] S.W. Song, G.V. Zhuang, P.N. Ross, Proceedings of the 204th Meeting of The Electrochemical Society, Abstract No. 410, Orlando, FL, October 12–16, 2003.